6338–6352 *Nucleic Acids Research, 2012, Vol. 40, No. 13* *Published online 26 March 2012*
doi:10.1093/nar/gks261

The mechanics behind DNA sequence-dependent properties of the nucleosome

Eugene Y. D. Chua, Dileep Vasudevan, Gabriela E. Davey, Bin Wu and Curt A. Davey*

Division of Structural and Computational Biology, School of Biological Sciences, Nanyang Technological University, 60 Nanyang Drive, Singapore 637551, Singapore

Received January 17, 2012; Revised March 6, 2012; Accepted March 8, 2012

ABSTRACT

Chromatin organization and composition impart sophisticated regulatory features critical to eukaryotic genomic function. Although DNA sequence-dependent histone octamer binding is important for nucleosome activity, many aspects of this phenomenon have remained elusive. We studied nucleosome structure and stability with diverse DNA sequences, including Widom 601 derivatives with the highest known octamer affinities, to establish a simple model behind the mechanics of sequence dependency. This uncovers the unique but unexpected role of TA dinucleotides and a propensity for G|C-rich sequence elements to conform energetically favourably at most locations around the histone octamer, which rationalizes G|C% as the most predictive factor for nucleosome occupancy *in vivo*. In addition, our findings reveal dominant constraints on double helix conformation by H3–H4 relative to H2A–H2B binding and DNA sequence context-dependency underlying nucleosome structure, positioning and stability. This provides a basis for improved prediction of nucleosomal properties and the design of tailored DNA constructs for chromatin investigations.

INTRODUCTION

Nucleosome positioning and occupancy underlie regulation of the genome (1,2), yet in contrast to sequence-specific DNA binding proteins, core histones have evolved to largely minimize sequence dependency in the nucleosome. Nonetheless, the tight wrapping around the histone octamer gives rise to an indirect readout of the DNA, whereby sequence-dependent attributes contribute to the free energy of nucleosome formation in the absence of base-specific protein contacts (3–6). Together with other factors like chromatin remodelling activities, the sequence dependency influences nucleosome dynamics and positioning, which contribute to genomic regulation by inhibiting or facilitating access to target DNA and protein sites. Although many, sometimes conflicting, models have been proposed in the past, the general attribute of %G|C content has recently emerged as the most decisive factor for predicting nucleosome occupancy *in vivo* (7,8), and yet the basis for this relationship is not obvious.

Structural and thermodynamics studies have shown that the sequence dependency of histone octamer binding arises from an interplay of sequence-specific DNA conformation and flexibility with the orientation of the major and minor grooves relative to the histone binding sites (3,5,6,9,10). Although the cumulative effect of DNA sequence alterations on binding affinity over the entire histone octamer can be substantial, the contribution of individual nucleotide changes is generally too small to be measured experimentally. Moreover, unique behavioural features of the double helix in the nucleosomal state (5,11,12) and the lack of detailed structural information over diverse DNA sequences have precluded elucidating the rules governing positioning and stability. Here, we present a nucleosome crystal- and solution-state structure analysis with stability measurements over nine different positioning DNA fragments, which has revealed a set of unifying mechanical principles behind histone octamer affinity for the double helix.

MATERIALS AND METHODS

Nucleosome production, structure solution and analysis

Design of expression constructs for DNA fragment production and generation of NCP from recombinant

*To whom correspondence should be addressed. Tel: +65 6592 1549; Fax: +65 6791 3856; Email: davey@ntu.edu.sg
Present addresses:
Dileep Vasudevan, Disease Biology Unit, Novartis Institute for Tropical Diseases, 10 Biopolis Road, #05-01, Chromos, Singapore 138670, Singapore.
Bin Wu, Department of Biological Chemistry and Molecular Pharmacology, Immune Disease Institute, Harvard Medical School, Center for Life Science Building, 3 Blackfan Circle, Boston, MA 02115, USA.

The authors wish it to be known that, in their opinion, the first two authors should be regarded as joint First Authors.

© The Author(s) 2012. Published by Oxford University Press.
This is an Open Access article distributed under the terms of the Creative Commons Attribution Non-Commercial License (http://creativecommons.org/licenses/by-nc/3.0), which permits unrestricted non-commercial use, distribution, and reproduction in any medium, provided the original work is properly cited.

Table 1. Data collection and refinement statistics

Parameter	NCP-601L	NCP-TA2	NCP146b
Data collection[a]			
Space group	$P2_12_12_1$	$P2_12_12_1$	$P2_12_12_1$
Cell dimensions *a*, *b*, *c* (Å)	106.5,109.5,174.8	106.5,109.9,182.3	105.5,109.3,175.9
Resolution (Å)	2.20–45.5 (2.20–2.32)	2.30–107 (2.30–2.42)	2.20–60.0 (2.20–2.32)
R_{merge} (%)	5.4 (50.7)	6.1 (17.4)	5.6 (48.4)
$I/\sigma I$	12.3 (1.6)	13.4 (3.6)	13.3 (2.2)
Completeness (%)	99.8 (99.0)	93.2 (69.4)	98.3 (89.9)
Redundancy	5.4 (3.4)	4.4 (2.2)	5.3 (3.6)
Refinement[b]			
Resolution (Å)	2.20–45.5	2.07–94.1	2.20–60.0
No. reflections	101 921	97 004	99 606
R_{work}/R_{free} (%)	25.7/28.9	24.1/26.6	23.2/27.5
No. of atoms	12 180	12 147	12 430
Protein	6068	6078	6015
DNA	5939	5939	5980
Solvent	173	130	435
B-factors (Å^2)	88	67	71
Protein	64	43	47
DNA	113	93	96
Solvent	76	50	56
RMSDs			
Bond lengths (Å)	0.010	0.009	0.010
Bond angles (°)	1.36	1.42	1.39

[a]X-ray wavelength used for data collection: 0.80 Å, NCP-601L, 0.9 Å, NCP-TA2, 1.07 Å, NCP146b. Values in parentheses are for the highest-resolution shell. [b]For NCP-TA2, additional reflections to 2.07 Å were used in refinement and for calculation of electron density maps (R_{merge} = 45.2% and completeness = 15.4% for the 2.07–2.18 Å shell).

Xenopus laevis histones were carried out as described previously (10,12,13). NCP-601L, NCP-TA2 and NCP146b crystallization, crystal stabilization, diffraction analysis and structural solution were conducted as reported before (10,12,14). Single crystal X-ray diffraction data were recorded at the Swiss Light Source (Paul Scherrer Institute, Villigen, Switzerland) using the PILATUS detector on beam line X06SA and a Mar225 CCD detector on beam line X06DA.

X-ray data were processed with MOSFLM (15) and SCALA from the CCP4 suite (16). Structural refinement and model building were carried out with routines from the CCP4 suite. NCP-601L, NCP-TA2 and NCP146b structures were solved by initial rigid body refinement using earlier NCP models (Table 1) (4,12,14). The NCP147, NCP146, NCP145, NCP-TA and NCP-601 structures that were used in analyses and comparisons were those previously reported (4,10,12,14).

For structural comparisons, NCP models were superimposed by least-squares fitting of the main chain atoms from the histone-fold domains (H2A, residues 23–91; H2B, residues 33–99; H3, residues 60–132; H4, residues 27–94). The identification of dinucleotide steps as major groove-inward, minor groove-inward and pressure points was established by the cosine of accumulated twist (CAT) values that indicate groove orientation relative to the histone binding surface (5). The accumulated twist values are calculated by summation, relative to the central base pair at the nucleosome 2-fold axis, of the local dinucleotide twist values associated with the step midpoints.

The phosphate groups comprising the binding platforms correspond to those from the nucleotide pairs on the inside of the superhelix that span the major-to-minor groove-inward transitions (black and orange phosphate pairs in Figure 1). The nucleotide numbers of the binding platform phosphate groups can be derived from the histone–DNA register assignments in Figure 1B: NCP145, chains I and J, −54, −53, −43, −42, −33, −32, −23, −22, −13, −12, −3, −2, 7, 8, 17, 18, 27, 28, 37, 38, 47, 48, 58, 59; NCP-601L, chains I and J, −54, −53, −44, −43, −34, −33, −24, −23, −13, −12, −3, −2, 7, 8, 17, 18, 28, 29, 38, 39, 48, 49, 58, 59; NCP146b, chain I, −54, −53, −44, −43, −34, −33, −24, −23, −13, −12, −3, −2, 7, 8, 17, 18, 28, 29, 38, 39, 48, 49, 59, 60, chain J, −55, −54, −44, −43, −34, −33, −24, −23, −13, −12, −3, −2, 7, 8, 17, 18, 28, 29, 38, 39, 48, 49, 58, 59; NCP147, chains I and J, −55, −54, −44, −43, −34, −33, −24, −23, −13, −12, −3, −2, 7, 8, 17, 18, 28, 29, 38, 39, 48, 49, 59, 60. For the double helix binding variability between NCP constructs analysis (Table 2), the positional deviation comparison sets entailed the 24 phosphorous atoms of the binding platforms from each H3–H4 tetramer and H2A–H2B dimer pair.

Dinucleotide step conformational parameters and reconstructions were obtained using 3DNA (18,19). Double helix axes and helical curvature values were calculated with Curves (20). Graphic figures were prepared with PyMOL (DeLano Scientific LLC, San Carlos, CA, USA).

Tyrosine fluorescence spectroscopy

Nucleosome stability was measured by monitoring the increase in fluorescence, which results from a loss in quenching of histone tyrosine residues by proximal DNA bases as DNA–histone interactions are disrupted (21–23).

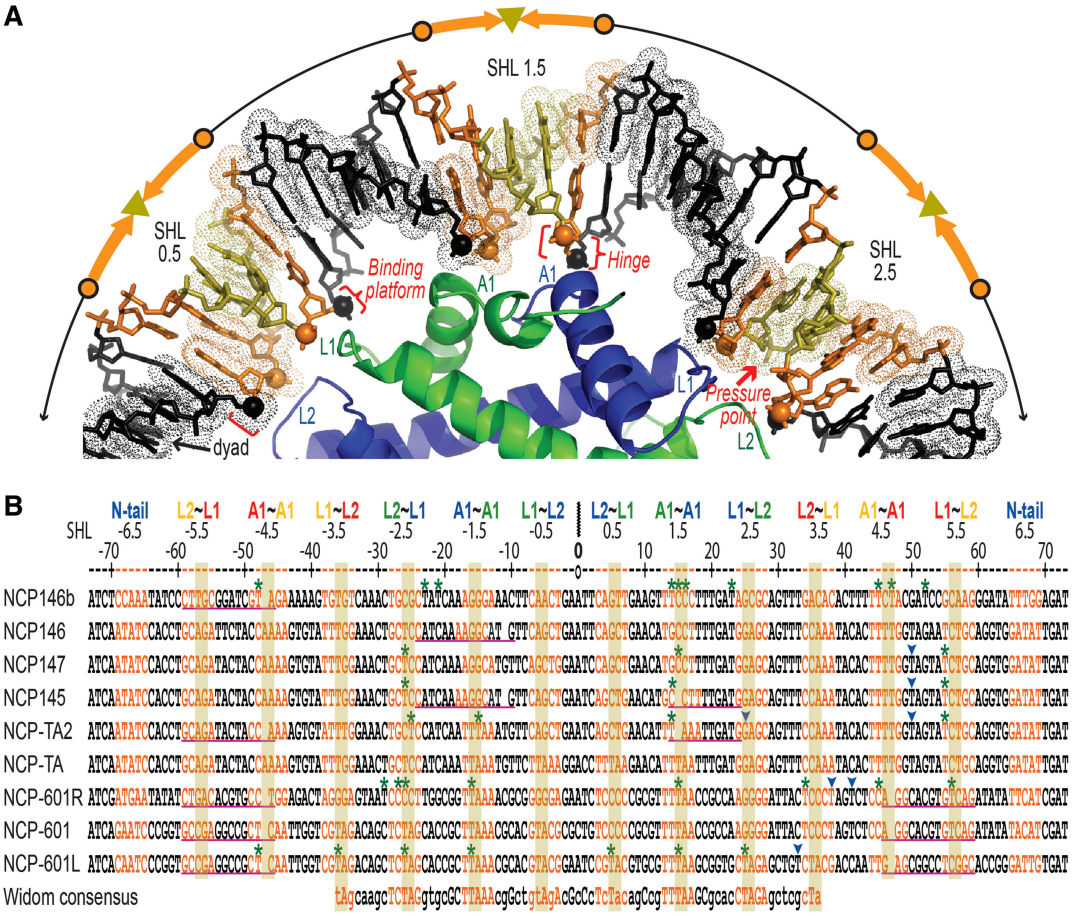

Figure 1. Double helix association, conformation and positioning on the histone octamer. (**A** and **B**) Minor and major groove-inward-facing regions are orange and black, respectively, with 'pressure points' at minor groove-inward centres highlighted gold. Histone proteins are blue, H3, green, H4, yellow, H2A and red, H2B (DNA-binding motifs: L, loop, A, α-helix). (A) Section of the NCP-601L crystal structure with phosphorous atoms of the 'binding platforms' shown as spheres. Bound single-strand regions act as a 'hinge', allowing conformational variation between different DNA sequences. (B) NCP constructs are arranged in order of increasing salt stability. Severe kinks at locations of DNA stretching around SHL ±2 or ±5 (magenta underlines), associated with a single base pair shift in histone-nucleotide register, are depicted as gaps in the sequence. DNA-permanganate reactivity hotspots in the nucleosomal state from footprinting analysis (six constructs) are indicated with green asterisks. Sites where the nucleosomal DNA shows reduced permanganate reactivity relative to the naked state are indicated with blue arrowheads. Capitalized bases in the Widom consensus sequence represent the most highly conserved nucleotides (17). The histone–DNA register assignments for NCP-601R and the Widom consensus sequence, for which crystal structures are not available, were inferred from the structures of NCP-601 and NCP-601L.

Fluorescence measurements were conducted with a Varian Cary Eclipse fluorescence spectrophotometer (Agilent Technologies, Santa Clara, USA) equipped with a temperature control unit. Samples of 0.5 μM NCP were allowed to equilibrate at 25°C in a buffer of 20 mM Tris (pH 7.5), 1 mM EDTA, 1 mM dithiothreitol and NaCl ranging in concentration from 0 M to 2.6 M. Fluorescence readings were taken at 20°C with samples in Teflon stopper cuvettes having 1-cm path length. Tyrosine fluorescence was measured by the emission at 306 nm through excitation at 275 nm.

Fluorescence measurements were carried out in triplicate and values for each data set were placed on a relative scale by setting the minimum and maximum values over the 0–2.6 M range to 0 and 1, respectively. The three normalized data sets for each construct type were then merged into one by averaging. Optimized sigmoidal profiles were fit to the merged data sets using OriginPro 8.1 (OriginLab Corp., Northampton, MA, USA), from which 50% dissociation points with respect to NaCl concentration were derived.

DNA distortion analysis by permanganate footprinting

Samples of 2.5 μM DNA or NCP in a buffer of 20 mM K-cacodylate (pH 6.0) were incubated with 1 mM $KMnO_4$ in the dark for 60 min at room temperature. A 10% molar excess of dTTP to $KMnO_4$ was added to the samples followed by incubation for 15 min to quench the reactions. Samples were subsequently treated with the addition of NaCl solution to a final concentration of 2 M, followed by phenol–chloroform extraction and ethanol precipitation of the DNA, which was then 5′ end-labelled with polynucleotide kinase. Thermally induced strand cleavage at $KMnO_4$-modified bases was effected by 30 min incubation of 10 μl samples at 99°C, followed by a further 30 min incubation after addition of 100 μl of 10%

Table 2. Variability in double helix binding by the H3–H4 tetramer and H2A–H2B dimers

Histone Sites		NCP147	NCP-601L
NCP-601L	H3–H4	0.48 ± 0.23	–
	H2A–H2B	1.16 ± 0.62	–
NCP145	H3–H4	0.48 ± 0.28	0.48 ± 0.25
	H2A–H2B	0.37 ± 0.17	1.11 ± 0.54
NCP146b	H3–H4	0.35 ± 0.19	0.57 ± 0.33
	H2A–H2B	1.43 ± 0.92	0.52 ± 0.27

Values (Å) are average differences in phosphate group positioning within the binding platforms between two NCP structures. The global average associated with all comparisons is 0.47 ± 0.25 Å for H3–H4 sites and 0.92 ± 0.50 Å for H2A–H2B sites.

Table 3. Comparison of permanganate reactivity between the highest and lowest stability NCP constructs

SHL	NCP-601L	NCP146b
±0.5	1.0 (0.1)	
±1·5	4.3 (0.4)	4.9 (0.3)
±2.0[a]		5.3 (1.7)
±2.5	11.1 (1.9)	
±3.5	4.1 (0.7)	
±4.5	2.1 (0.1)	3.7 (1.9)
±5.0[a]		1.8 (1.1)
Minor groove-inward	22.6 (3.3)	8.7 (2.2)
Major groove-inward[a]		7.0 (2.9)
Total	22.6 (3.3)	15.7 (5.1)

Values correspond to reactivity hotspot intensities in the nucleosomal state with corresponding values for the naked state in parentheses. [a]Note that two hotspot locations are at major groove-inward positions for NCP146b.
See Figure 1B for overview.

(v/v) piperidine with 50 mM EDTA (pH 8.0). Maxam–Gilbert purine sequencing standards (24) were prepared as markers. DNA fragments were resolved by denaturing PAGE (10% polyacrylamide, 8 M urea, 88 mM Tris–borate, 2 mM EDTA, pH 8.3), in which loaded quantities of DNA samples corresponded to approximately equal total radioactive counts.

The Quantity One program (Bio-Rad Laboratories) was used for intensity quantification of gel bands (Table 3). The reactivity hotspot intensities for the nucleosomal state (Figure 7B, lanes 3 and 9), and the corresponding locations in the naked DNA state (lanes 2 and 8), were placed on a relative scale by normalizing with respect to the band intensity associated with nucleotide 5 (SHL ±0.5) of NCP-601L (lane 3). For SHL sites containing more than one reactive nucleotide, normalized intensities were summed to yield the values given in Table 3.

RESULTS

Nucleosome structure with the highest affinity DNA sequences

Most nucleosome core particle (NCP) crystal structures have been based on a single type of human α-satellite sequence (25), but the discovery of DNA fragments with the highest known affinity for the histone octamer, by selection from a pool of synthetic random sequences (17,26), affords an opportunity to decipher the precise mechanics of DNA wrapping. Structures with the most widely used construct derived by this approach, the Widom 601 strong positioning sequence, have recently been solved and analysed (12,27,28), but they do not provide an unambiguous picture of the DNA conformation due to the non-palindromic nature of the fragment. To overcome the problem of orientational mixing of non-identical sequences between the two pseudo-symmetry-related NCP halves in the crystal, we generated palindromic derivatives of the left and right halves of the 601 sequence, 601L and 601R. We obtained a 2.2 Å resolution crystal structure of NCP assembled with 601L (NCP-601L; Table 1 and Supplementary Figure S1), although crystals of NCP-601R diffracted only very poorly. In combination with new high-resolution structures for NCP146b and NCP-TA2, which are composed of a distinct α-satellite sequence (4) and derivative, respectively, the histone–DNA register established for the three 601 and six centromeric constructs permits unprecedented insight into sequence versus position relationships in the nucleosome (Figure 1).

Alignment of the highest affinity sequences derived by SELEX allowed Widom and colleagues to predict a consensus sequence for maximum affinity histone octamer binding over the central 73 bp of the nucleosome (this approach apparently did not allow full optimization of the outer H2A–H2B binding sites; Figure 1B) (17). Our 601L is very similar to this consensus sequence, and in fact, NCP-601L displays extraordinary salt stability, which is substantially above that of the parent 601 particle (NCP-601; Figure 2 and Supplementary Figure S2). Conversely, the stability of NCP-601R is significantly reduced relative to NCP-601, although it is still above that of the α-satellite-based NCPs, which all form a cluster with similar stabilities.

The general attributes that appear to endow the 601L (like the consensus) sequence with exceptional histone octamer affinity have been previously outlined (12). These include the presence of the most flexible dinucleotide type, TA (29), at minor groove-inward positions where DNA distortion is energetically most challenging (30,31) and G|C-rich elements, which are predisposed to major groove bending/compression, at major groove-inward positions. Moreover, 601L and the other 601 sequences contain TTTAA elements at minor groove-inward locations situated 1.5 double helix turns from the nucleosome centre (SHL ±1.5). This coincides with the most stringent singular positioning signal in the nucleosome (9), whereby extreme narrowing of the minor groove is required (10), and α-satellite derivatives engineered with TTTAA elements at SHL ±1.5 (NCP-TA and NCP-TA2) also display increased stability over their parent constructs (Figure 2 and Supplementary Figure S2). Nonetheless, the reason why TA steps in the highest affinity sequences occupy such uniquely defined positions within the different minor groove-inward locations (Figure 1B) is not clear. Moreover, as apparent from the

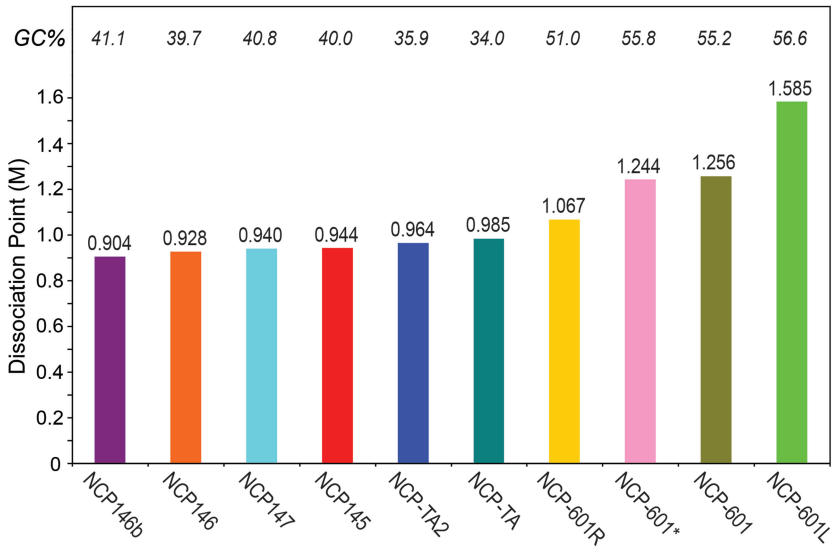

Figure 2. DNA sequence-dependent salt stability of the nucleosome core. Dissociation points correspond to the midpoints of NaCl-induced DNA–histone dissociation measured by tyrosine fluorescence spectroscopy. NCP-601* is composed of a 147 bp Widom 601 fragment (12).

crystal structure of NCP-601L, the TA elements do not take up the strongly kinked conformations expected based on the behaviour of highly flexible CA = TG dinucleotides in the earlier α-satellite structures (Figures 3 and 4). Additionally, the high stability of NCP-601R in spite of having GGG(G) elements over six of the eight minor groove-inward locations around the nucleosome centre (Figure 1B) blatantly conflicts with the general preference of G|C sequences to take up the opposite orientation of major groove-inward (3,6,17).

Mechanical model for DNA sequence dependency

Previous models for the sequence-dependent mechanics of wrapping in the nucleosome have been based on the contribution of specific DNA conformational parameters, foremost base pair step roll and slide (Figure 3A for an illustration of the six dinucleotide step parameters), towards generation of the superhelix (5,32). However, this is only an indirect description that does not address the underlying localized constraints on double helix structure, which moreover arise from a form of protein association that is unique to the nucleosome. Histone binding involves mainly interaction with the inward-facing phosphodiester backbone. In particular, for every turn of the double helix there are four phosphate groups that are in closest proximity to the histone octamer surface, encompassing the most extensive protein–DNA interactions. The phosphorus atoms of these four phosphate groups, designated as the 'binding platform', lie roughly in a plane and show the least variation in position between different DNA sequences (Figures 1A and 5). Thus, the binding platform represents the most constraining feature of histone association, which requires a very narrow minor groove for both DNA strands to fit on the protein surface. Correspondingly, the major groove must be narrow where it faces inward in order for both strands to fit onto adjacent binding platforms. Furthermore, the two sides of the binding platforms each act like a 'hinge', which allows freedom in the positioning of the opposing, unbound DNA strand (Figures 1A, 5 and 6). This attribute permits substantial conformational variation between different DNA sequences, limiting the sequence dependency of the nucleosomal system.

In comparing double helix conformation between the three NCP crystal structures having the least DNA sequence similarity (NCP147, NCP146b and NCP-601L), which also display the same histone-nucleotide register over the central ~100 bp due to the absence of DNA stretching (Figures 1B and 6 for illustrations of stretching) around the SHL ± 2 locations, it is evident that histone association both imposes substantial constraints and allows a significant degree of freedom (Figures 3 and 5). The conformational freedom relates largely to swivel-like alterations about the hinges while upholding the constraints of the binding platforms, and the most striking example of this corresponds to distinctions between NCP145 and NCP147, which, in spite of near DNA sequence identity, differ dramatically in double helix structure over the SHL ±1 to SHL ±2 regions (Figure 6). Whereas NCP147 displays smooth bending over these regions, DNA stretching occurring in NCP145 is accompanied by extreme kinking into the major or the minor groove. These dramatic conformational differences give rise to a distinct distribution of double helix curvature between hinges, but coincide nonetheless with nearly identical phosphate group positioning within the H3–H4 binding platforms. On the other hand, sequence-specific differences in histone binding over the other region of potential DNA stretching, SHL ±4.5 to SHL ±5.5, have been reported previously (4,27), and a substantial variability in H2A–H2B association over this location is evident from comparison of the most diverse NCP constructs (Figures 3 and 5).

The H3–H4 tetramer dominates sequence dependency

Analysis of non-covalent interactions in the NCP crystal structure (4) and mechanical unzipping of the nucleosome (33) indicated that DNA–histone interaction strength is greater over the H3–H4 tetramer compared to the H2A–H2B dimers. This suggests that the tetramer may impose stronger constraints on DNA conformation, which in turn could disproportionately affect stability and positioning. When we analyzed here variations in phosphate position within the binding platform between the NCP structures with the most diverse DNA sequences and DNA stretching configurations, we found that there is in general substantially greater conformational freedom over the H2A–H2B versus the H3–H4 sites (Table 2). This indicates that the DNA sequence content associated with the H3–H4 binding surface would have a dominant influence on positioning and stability. Correspondingly, H3–H4 association could impose discrimination between the two distinct forms of minor groove bending. However, examples of isolated kinks versus smooth bending accompanied by alternating shift, and indeed mixtures of the two, can be seen to substitute for one another at individual H3–H4 and H2A–H2B sites depending on the DNA sequence (Figures 3 and 6). Thus, the double helix seems free to adopt one of a subset of favourable conformational modes within the confines of the binding

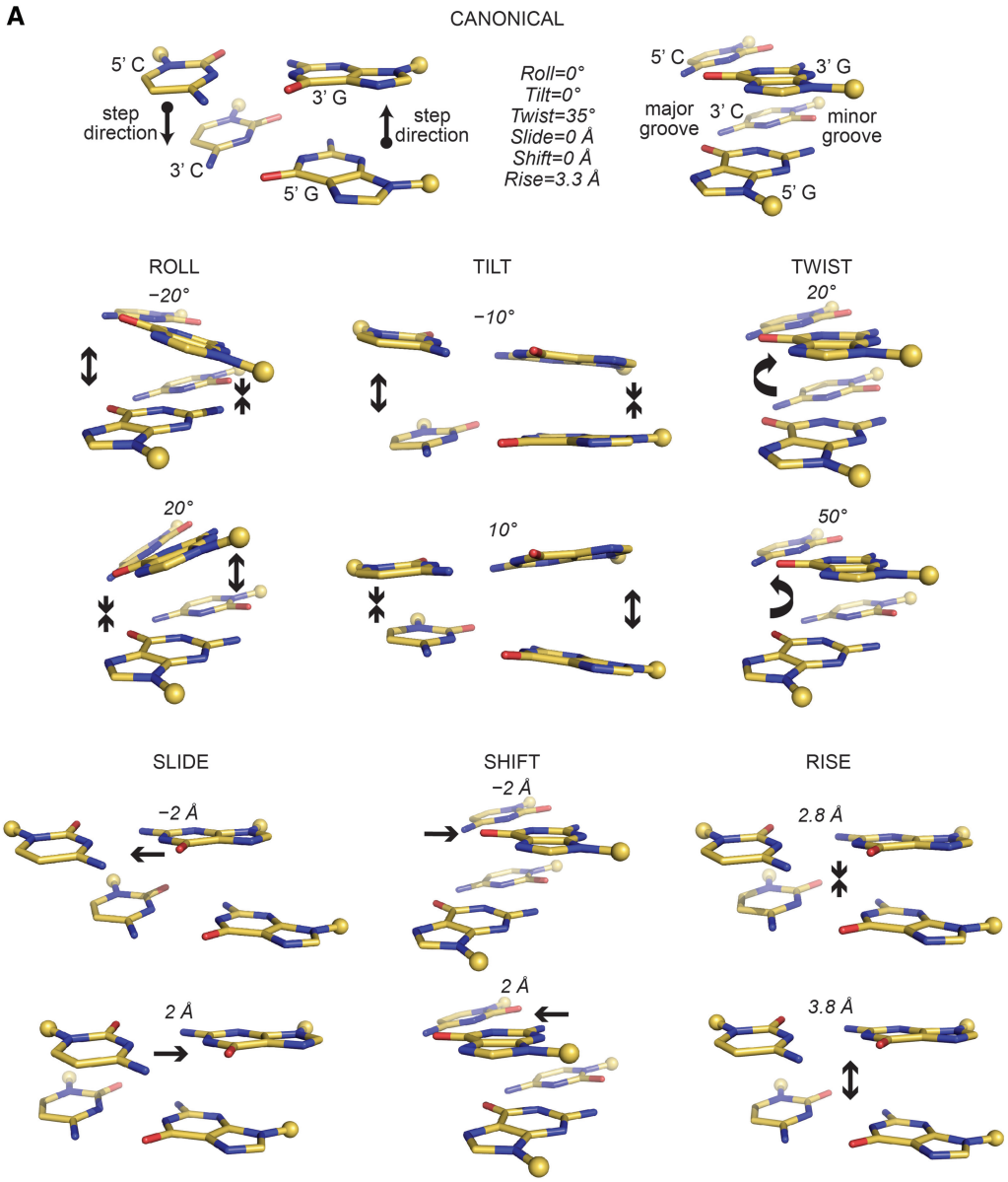

Figure 3. Dinucleotide step parameters. (**A**) Illustration of the six degrees of freedom for DNA structure at the base pair step level. (**B**) Dinucleotide step values for NCP-601L (blue) and NCP147 (green) averaged over one particle half and for the two particle halves of NCP146b (red and yellow; NCP146b displays a distinct DNA–histone register in each half). Dinucleotide steps in major groove-inward sections in addition to the flanking major-to-minor groove-inward interface steps have a grey shaded background. The four dinucleotide steps in each minor groove-inward section have a white background with a gold shading indicating the step located at the pressure point.

(continued)

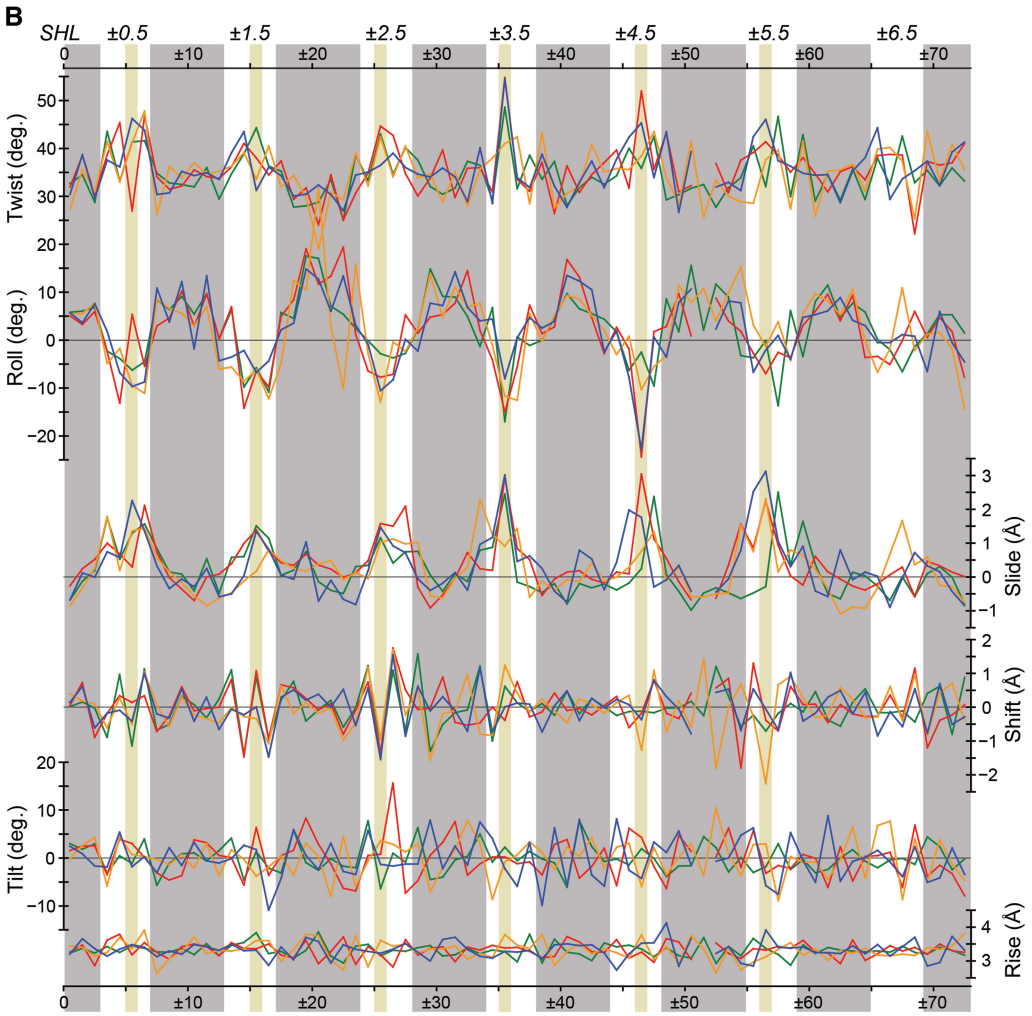

Figure 3. Continued.

platforms. At the same time, however, there appear to be histone-specific distinctions that predispose a particular bending mode. This is most evident at the SHL ± 2.5 H3–H4 site that consistently displays a striking alternating shift pattern, wherein defined histone interactions could select for the distinct BII phosphate backbone configuration, which is notably enriched by this conformational mode (Figures 3 and 4) (5).

Minor groove-inward regions dominate sequence-dependent attributes

As suggested previously (10) and consistent with recent computational studies (30,31), our data here illustrate that the sequence content of minor groove-inward sections dominates positioning and stability. Major groove-inward sections display greater conformational freedom in the crystal structures and their sequence content is more variable (Figures 1B, 3 and 5). Although systematically G|C-rich, these regions are less conserved in the highest affinity sequences compared to the minor groove-inward sections (see Widom consensus; Figure 1B). Moreover, the major groove-inward sections of the α-satellite sequences are in fact A|T-rich, although highly flexible, centrally located CA = TG and TA dinucleotides are likely a stabilizing factor. Nonetheless, the optimal major groove-inward sequences consist mostly or purely of G|C nucleotides and the ideal motifs apparently correspond to alternating dinucleotide types, wherein the flexibility inherent in CG and GC steps is seemingly stabilizing.

In contrast to the nominal conformational character of major groove bending in the nucleosome core, the minor groove-inward sections display specialized modes of distortion (5,10). Although the TA dinucleotides in the NCP-601L structure coincide with the points of maximal bending into the minor groove, the bending mode over the different sites is mostly smooth with low curvature, and even in the case of the kinking observed at SHL ± 3.5, the magnitude (of roll) is much reduced relative to that at CA = TG dinucleotides in the α-satellite constructs (Figure 3). On closer inspection, however, the TA elements display unusual distortions not obvious from the dinucleotide step parameters alone (Figure 4). This is consistent with permanganate footprinting analysis of

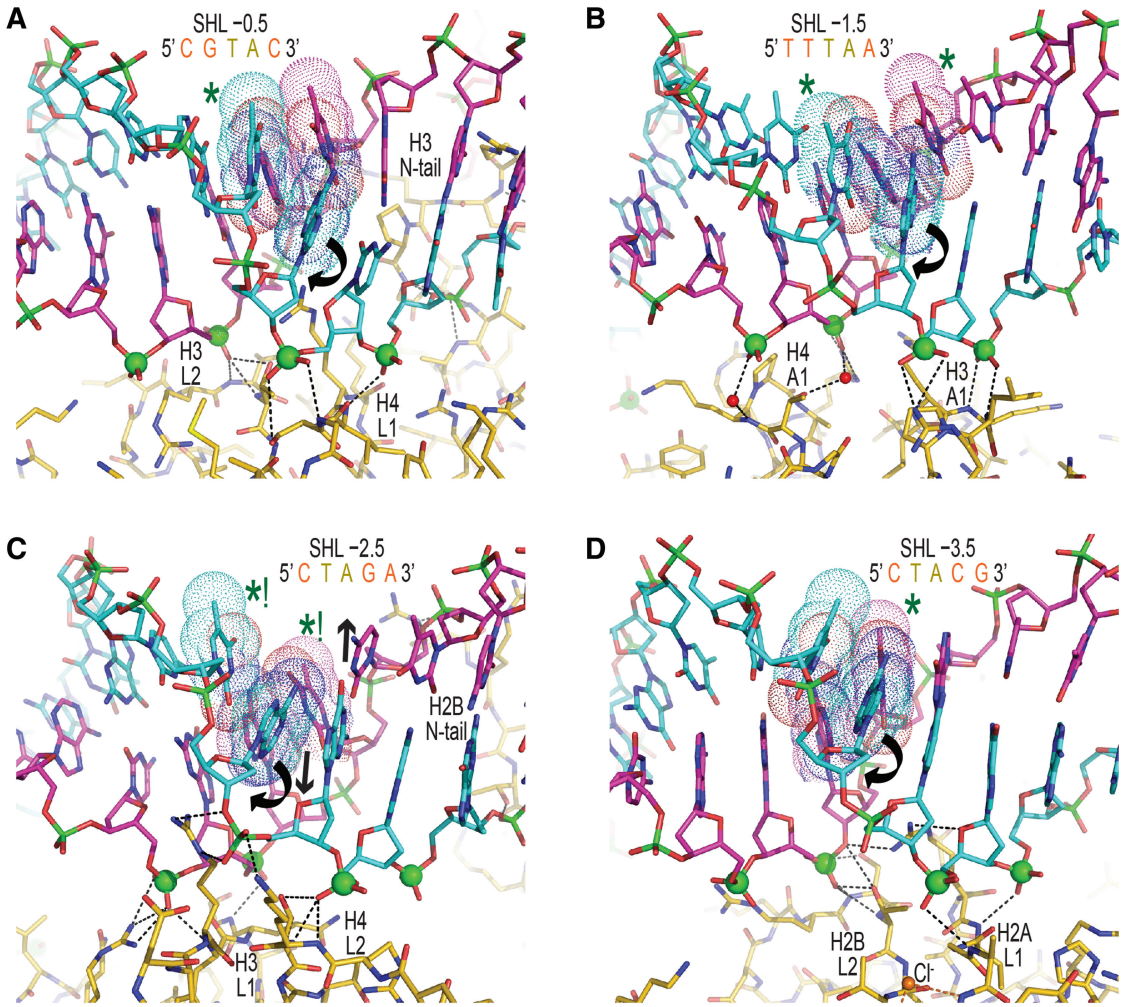

Figure 4. DNA binding and structure over TA elements in NCP-601L. (**A–D**) TA dinucleotides (bases, space filling dots) are situated at the pressure points of the centrally located histone binding sites, where they display a diversity in conformational distortions. Rotational dislocation of bases within the TA step (curved arrows, only front strand shown for clarity) permits unabated compression of the minor groove for fitting of the binding platform (phosphorous atoms, spheres) to the histone surface. DNA–histone hydrogen bonds appear as black dashed lines. Permanganate reactivity hotspots are designated with asterisks, whereby that at SHL ±2.5 is by far the most prominent as a consequence of extreme base unstacking promoted by base pair displacement into the minor and major grooves via shift (C, arrows). Note that shift is also the primary DNA structural parameter influencing platinum drug reaction, since it dictates solvent access to the major groove edge (14).

naked and nucleosomal DNA in solution, which reveals sites of double helix distortion by virtue of elevated reactivity of unstacked thymine (primary intrinsic reactivity) and cytosine (secondary intrinsic reactivity) bases towards permanganate ion (Figure 7 and Supplementary Figure S3) (9,34). The NCP DNA displays pronounced reactivity hotspots relative to the naked state, and almost all of these coincide with minor groove-inward sections (Figures 1B, 4 and 8). This emphasizes the primary importance of the sequence content over these sites, since the DNA is distorted greatest from its naked state conformation (Table 3). Furthermore, the most prominent hotspots coincide with H3–H4 tetramer binding sites, in particular SHL ±1.5 and SHL ±2.5, which are indeed the most conserved regions in the Widom consensus sequence.

The origin of the special structure and function of the TA dinucleotides becomes clear by considering association of the binding platform. The conspicuous localization of TA at defined points of the minor groove-inward sections in the 601 and consensus sequences coincide with the positions at which the minor groove is most directly facing inward and, consequently, under the greatest pressure to contribute to superhelix formation through distortions into the minor groove (Figures 1 and 4). These 'pressure points' are seemingly invariant with respect to the DNA sequence since they also coincide with the most inward facing dinucleotide step positions of NCP147, which notably lacks TA at any of the minor groove-inward facing sections (Supplementary Figure S4). In contrast to the more conservative behaviour of other dinucleotide types at the pressure points (DNA stretching notwithstanding), individual base pairs within the TA steps are distorted by extreme propeller twisting and other deformations that cause unstacking and diminish Watson–Crick

bonding (Figure 4 and Table 4). This kind of behaviour for A•T base pairs was described in a recent analysis (28) of the NCP-601 structures (12,27). For the eight TA steps situated at the pressure points in the NCP-601L model, we find that, with the exception of propeller twist values that can reach −48° and average −25 ± 14°, the five other base pair parameters are on average close to ideal (near zero values; Table 4). This contrasts with the behaviour at the corresponding pressure point steps in NCP147 and NCP146b, which are non-TA and have a significantly greater tendency for a particular directionality of base pair distortion. What is remarkable for the TA step base pairs in NCP-601L is that they display a degree of distortional variation that is well above that of the corresponding base pairs of NCP147 or NCP146b.

The pronounced dinucleotide step and base pair distortions associated with the pressure point TA steps results in a nucleotide from one or both DNA strands being to some extent dislocated from the double helical stack, which serves to collapse the minor groove for fitting of the binding platform to the histone surface. The type of distortion required depends critically on the intrinsic conformational preference of the sequence element, whereby the intrinsically narrow TTTAA motifs at SHL ± 1.5 display only minimal bending into the minor groove (Figures 1A, 3 and 4). In fact, when NCP145 is modified to have these motifs (yielding NCP-TA2; Figure 1B), such that the TA step is placed where the extreme stretch-induced kink was present at the SHL ± 1.5 GG = CC in NCP145, the resulting kinking is much reduced because the binding platform would otherwise be overly narrow (Figure 9). In this regard, the most severe kinks at minor groove-inward regions occur at sequence elements having G|C character, and therefore

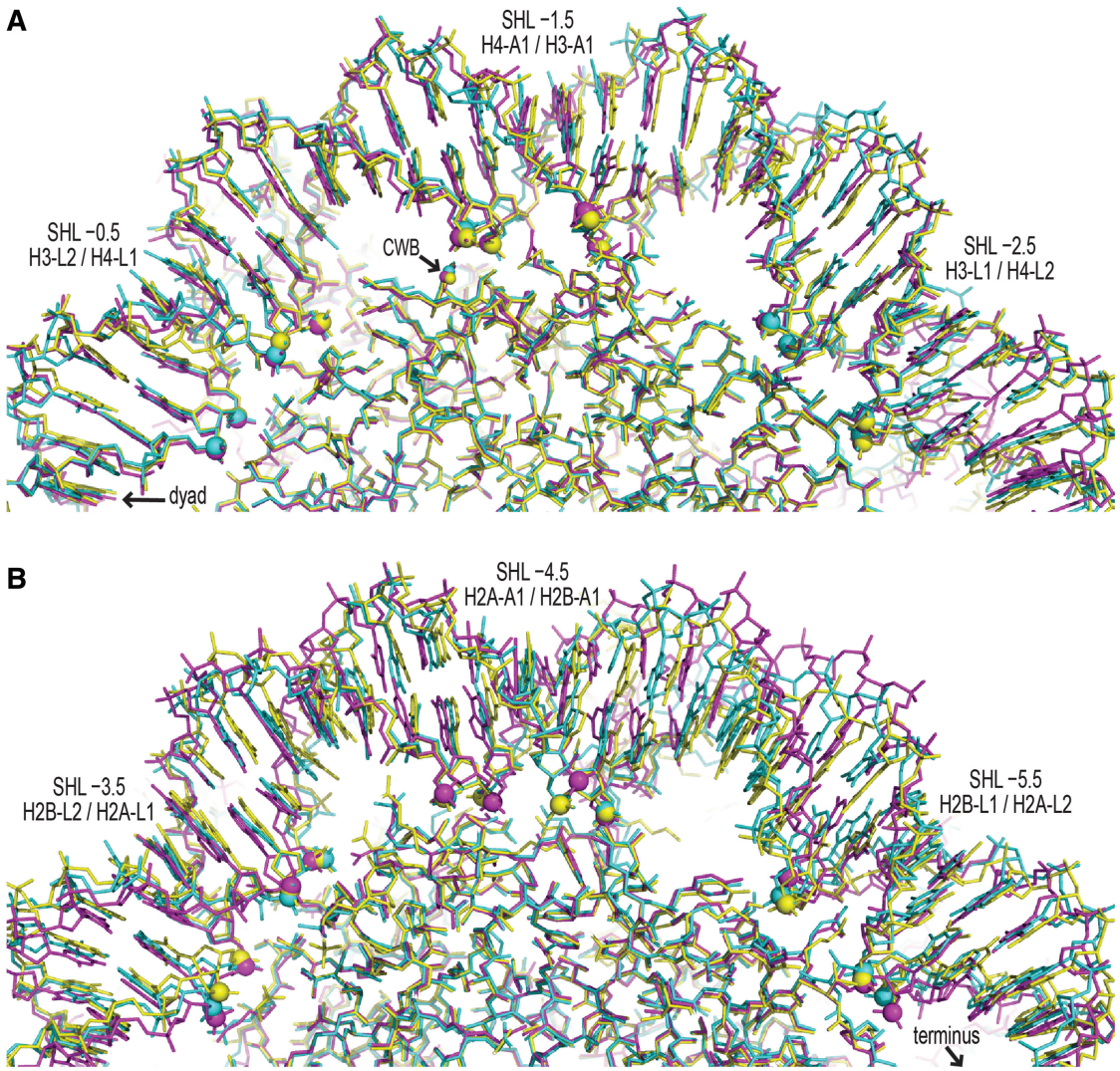

Figure 5. Constraints of histone binding on double helix structure and site-dependent variation between different DNA sequences. (**A–D**) The structures of NCP147 (magenta), NCP146b (yellow) and NCP-601L (cyan) were superimposed via the histone-fold regions of the octamer (DNA binding motifs: L, loop, A, α-helix). The phosphorous atoms of the binding platforms appear as large spheres, and water molecules mediating a conserved DNA–histone hydrogen bond bridge are shown with small spheres (A and C; CWB). (A and C) H3–H4 tetramer binding sites. (B and D) H2A–H2B dimer binding sites.

(continued)

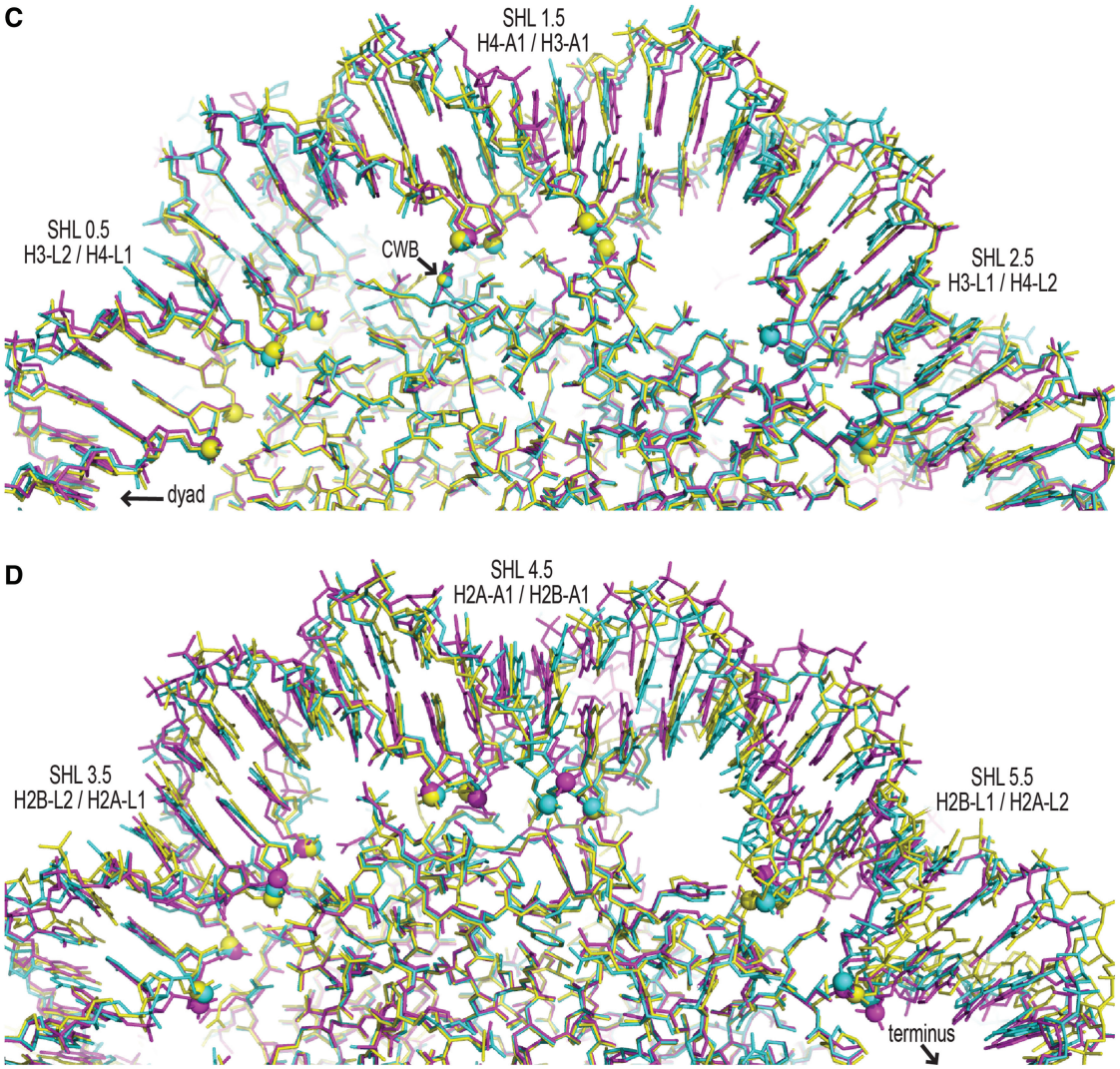

Figure 5. Continued.

arise from a combination of DNA positioning preferences and local groove narrowing requirements that together determine the incidence of double helix stretching (Figure 1B).

DISCUSSION

DNA sequence-dependent nucleosome positioning and stability are governed by the energetic cost of deforming the double helix to fit the histone binding surface. In this regard, the histone octamer provides a roughly rigid scaffold to which the DNA must adapt for association (Figure 5). The structural constraints on the double helix are greatest over the H3–H4 tetramer binding sites, and the conformational challenges towards deformation are maximal for minor groove-inward facing regions, which make the DNA sequence at these locations dominate histone octamer affinity. Considering our data here and previous findings on histone site-dependent contributions to nucleosome positioning and stability, as well as the variation in degree of nucleotide conservation in the Widom consensus sequence (9,10,17) (Figure 1B), allows us to infer a tentative ranking for the relative importance of the different minor groove-inward sections towards histone octamer affinity: SHL ±1.5 > SHL ±2.5 > SHL ±0.5 > SHL ±3.5 > SHL ±4.5 > SHL ±5.5.

The interplay between DNA sequence, deformation and affinity for the histone octamer can be illustrated by analysis of the constructs with highest and lowest stability in our study, NCP-601L and NCP146b, which display a nearly 2-fold difference in salt stability (Figure 2). For NCP-601L, permanganate reactivity hotspots are limited to the four different TA dinucleotide sites surrounding the nucleosome centre (SHL ±0.5, ±1.5, ±2.5, ±3.5) in addition to the location of stretch-induced extreme kinking at the GA = TC step of SHL ± 4.5 (Figures 1B and 7). Positioning of TA steps at these dominant pressure points allows for a minimum distortion energy, because TA is the loosest stacking dinucleotide step in conjunction with the weaker base pairing interaction for A•T versus

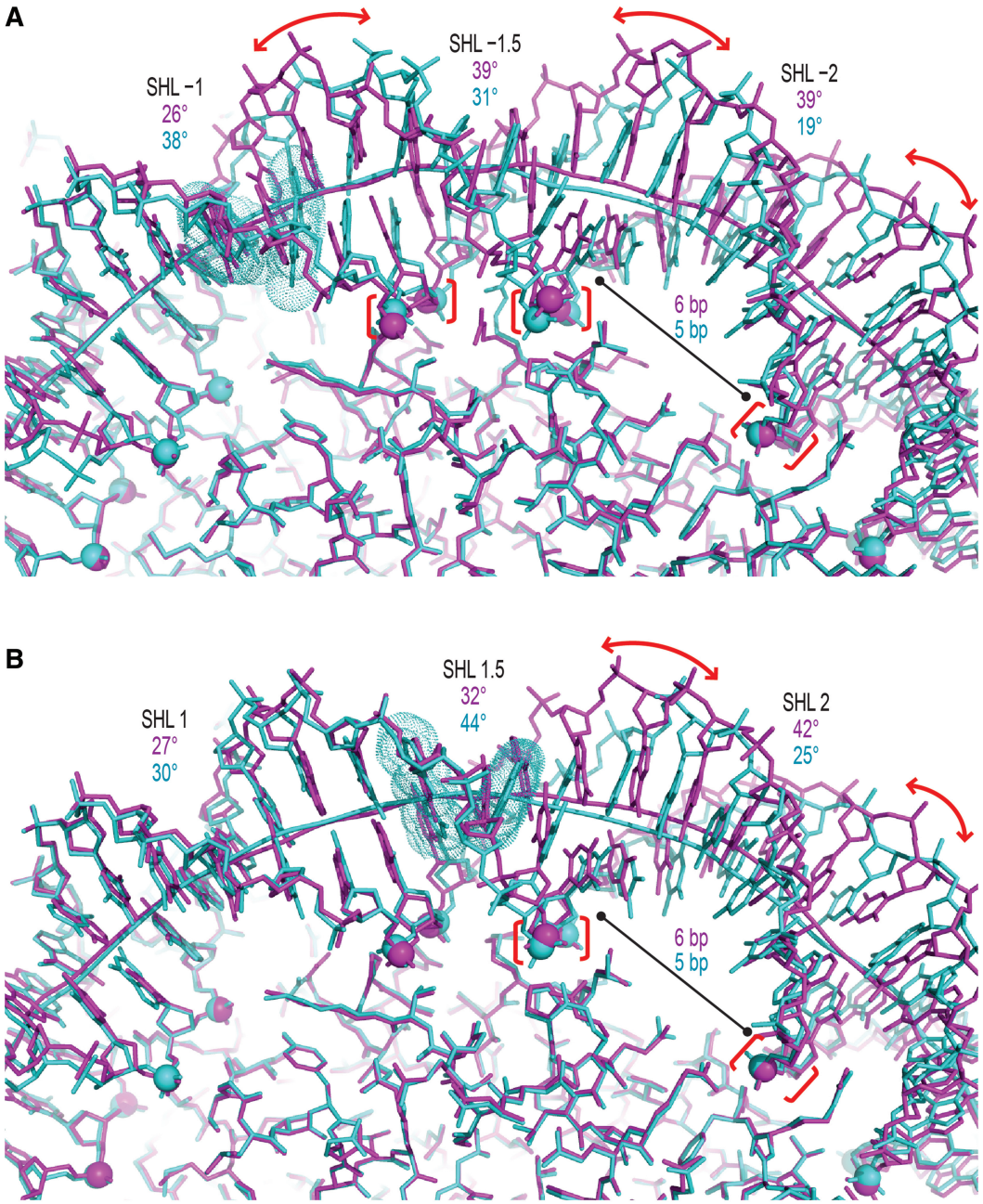

Figure 6. DNA single-strand histone attachment points act as hinges to allow double helix conformational freedom. (**A** and **B**) DNA stretching around SHL ± 1 to SHL ± 2 in NCP145 (cyan) gives rise to substantial structural differences compared to NCP147 (magenta), which displays no stretching but is composed of a DNA with nearly identical sequence. Histone association with the binding platforms (phosphorous atoms, spheres) is very similar between the two constructs, whereby the extreme stretch-associated kinking in NCP145 (bases, space-filling dots) at either SHL −1 (A; CA = TG, roll = 38°, rise = 5.0 Å) or SHL 1.5 (B; GG = CC, roll = −52°, rise = 5.7 Å) is accommodated largely by swivel-like repositioning of the double helix (curved arrows) about the hinges (brackets). This results in a distinct distribution of helix axis (tubes) curvature between the major and minor groove-inward regions (values shown).

G•C (29). In fact, the next loosest stacking step, CA = TG, has nearly twice the stacking energy as TA and moreover contains a G•C pair. In this regard, as gleaned from the NCP structures and permanganate reactivity, the TA step is free to distort in a great variety of ways, at both the step and base pair levels, for low energy fitting to the octamer. In fact, the overall degree of DNA distortion in the nucleosomal state relative to the naked state, estimated by the differential permanganate reactivity, is larger for NCP-601L compared to NCP146b (Table 3). Therefore, the deformation of the 146b DNA from fitting on the octamer is actually less than that of the 601L DNA, while the resulting energetic cost of distortion must be substantially greater because of the suboptimal 146b sequence. Moreover, in contrast to NCP-601L and the other constructs, NCP146b displays reactivity

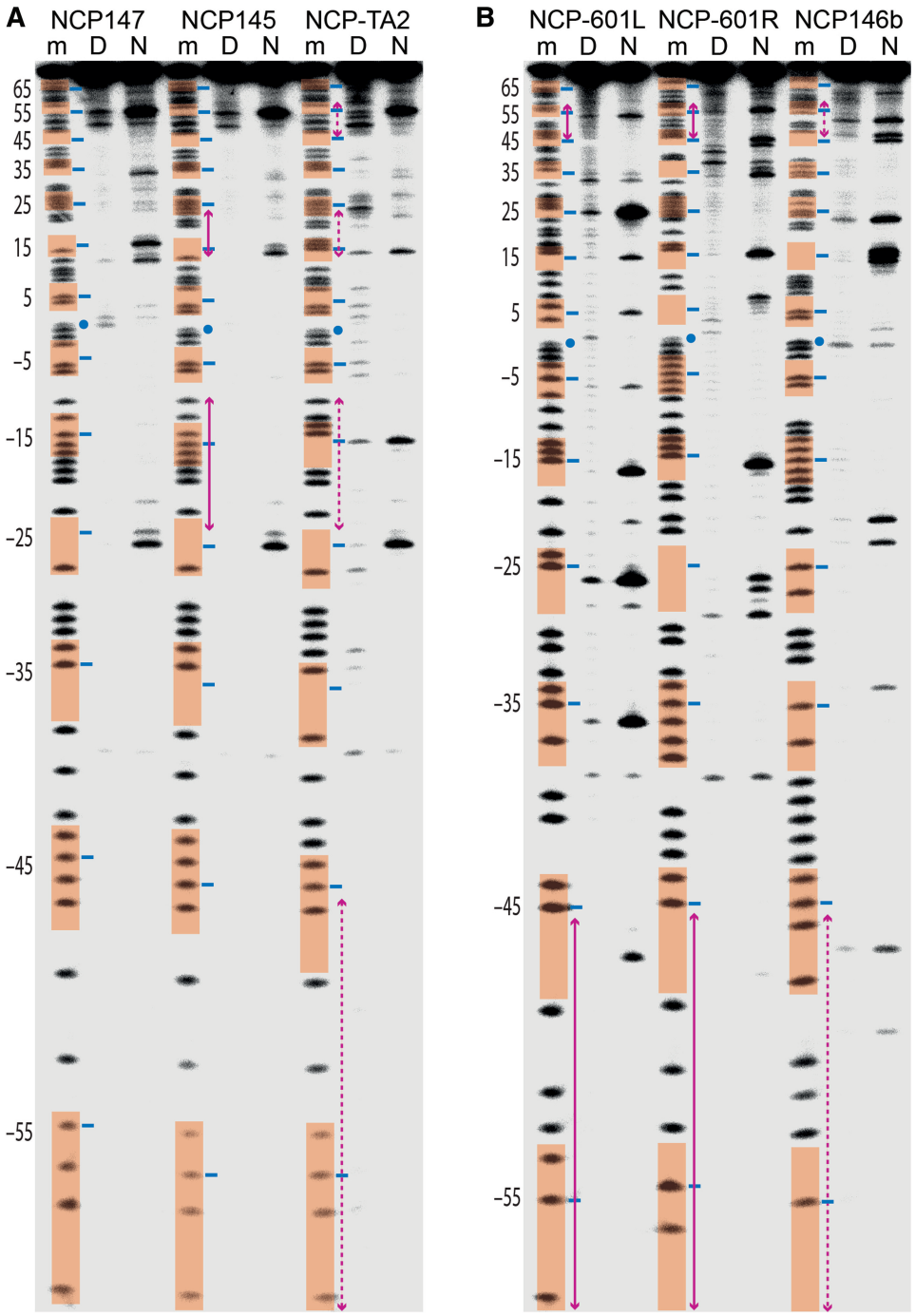

Figure 7. $KMnO_4$ footprinting reveals DNA context-dependent distortions. (**A** and **B**) DNA samples, comprising six different constructs, correspond to purine sequencing standard (m) or naked DNA (D) and NCP (N) that were subjected to permanganate reactivity analysis. Minor groove-inward-facing nucleotides (highlighted in orange), regions of DNA stretching (magenta arrows; dashed for mixed stretched and non-stretched configurations) and the central nucleotide (blue dot) are based on the crystal structure assignments (Figure 1B).

hotspots also at SHL ±2 and ±5, which correspond to pronounced deformations relative to the naked state at major groove-inward regions (Table 3). In this sense, there would be an additional energetic expenditure to deform A|T elements of 146b for major groove bending—a type of conformation that is easily accessible to most G|C sequences.

Although TA dinucleotides are ideal for the mechanics required at pressure points, the optimal sequence context can vary over the different histone binding sites. This is perhaps most evident at the most stringent motifs, SHL ±1.5 and ±2.5, for which the sequence elements are identical between NCP-601L and the Widom consensus sequence and apparently optimal. The permanganate

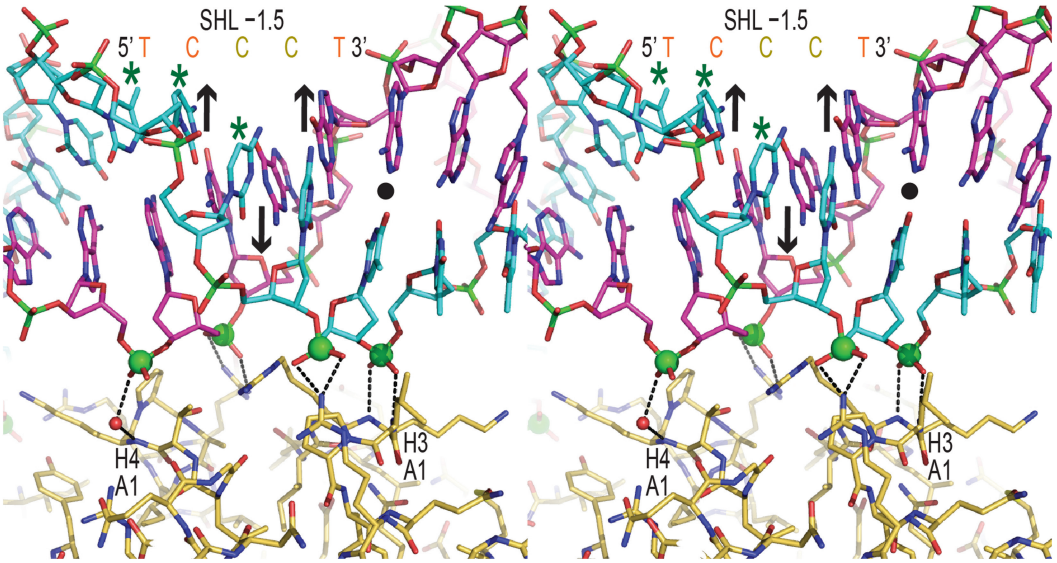

Figure 8. G|C-rich elements can undergo energetically favourable distortions at minor groove-inward positions by adopting specialized conformations. Stereo view of the AGGGA (=TCCCT) motif at the SHL − 1.5 location in NCP146b, which displays smooth bending with pronounced alternating displacement of base pairs into the minor groove (downward-pointing arrow and filled circle indicating displacement away from the viewer) and major groove (upward-pointing arrows) via fluctuating shift. DNA–histone hydrogen bonds appear as black dashed lines. Permanganate reactivity hotspots are designated with asterisks.

Table 4. Base pair parameters of dinucleotides at pressure points

Parameter	NCP-601L	NCP146b	NCP147
Shear (Å)	−0.08 ± 0.48	0.08 ± 0.42	−0.22 ± 0.23
	−1.12, 0.76	−0.51, 1.01	−0.60, 0.28
Stretch (Å)	0.03 ± 0.20	−0.15 ± 0.20	−0.12 ± 0.13
	−0.31, 0.39	−0.51, 0.23	−0.38, 0.26
Stagger (Å)	−0.16 ± 0.35	0.41 ± 0.35	0.30 ± 0.29
	−0.78, 0.41	−0.01, 1.28	−0.48, 0.75
Buckle (°)	0.8 ± 9.3	4.1 ± 7.8	2.7 ± 6.0
	−10.2, 23.4	−11.0, 13.6	−10.4, 18.2
Opening (°)	1.0 ± 4.5	−1.7 ± 4.0	−1.1 ± 2.8
	−6.0, 11.0	−8.6, 5.0	−7.3, 2.9
Propeller (°)	−24.8 ± 13.8	−19.0 ± 10.9	−17.1 ± 10.5
	−48.2, −0.8	−35.7, −1.9	−37.2, 2.9

Values are averages (upper entry) and minima/maxima (lower entry) associated with the eight dinucleotide steps at the pressure points of SHL ±0.5, ±1.5, ±2.5 and ±3.5. Shear and buckle values correspond to all purine•pyrimdine base pairs placed in the same orientational frame.

reactivity of TA in the NCP-601L SHL ±2.5 CTAGA element is by far the greatest (Table 3), consistent with the tremendous base unstacking seen in the structure (Figure 4C). The TA reactivity of the SHL ±1.5 TTTAA element is the next strongest, but notably this site in the naked state has low reactivity, which denotes good stacking and absence of significant distortion, whereas the naked state CTAGA element displays substantial reactivity, indicating an intrinsically distorted structure. In this way, the TTTAA element is tailored to the extreme groove-narrowing requirements at SHL ± 1.5 (10), while CTAGA appears optimal for the extreme alternating shift pattern favoured at SHL ±2.5. The energetic cost of unstacking a dinucleotide from the double helix is governed by the identity of the flanking nucleotides, which for TA is minimal when N_1TAN_4 equals CTAG (29). In this regard, flanking AG = CT steps are not only ideal from the standpoint of the loosest stacking environment for TA (29), but also they provide the most shift-flexible context for an N_1TAN_4 tetranucleotide (35).

With the exception of the requirement for soft spots at every turn of the double helix best fulfilled by TA elements, the highest affinity sequences are decisively G|C-rich, with the 601L and Widom consensus composed of only 43.4 and 45.2% A|T nucleotides, respectively (Figure 2). This could help explain the correlation between G|C% and nucleosome occupancy *in vivo*, but maximizing histone octamer affinity by selection *in vitro* (17,26) represents the greater good of sequence space, and such sequences have not been identified in genomic analyses. In contrast, the contribution of DNA sequence towards nucleosome positioning *in vivo* appears to be largely governed by the lesser of available evils, which notably includes octamer exclusion from poly-A:T elements (1,2,36). Indeed, the fact that both minor and major groove-inward sections rich in either A|T or G|C nucleotides can yield well-positioning sequences (Figure 1B) would weaken generalized correlations, contributing to the lack of agreement between some positioning studies.

A key consideration behind the stabilizing effect of G|C content is the contribution of specific sequence elements that are of sub-optimal favourability with respect to minor groove bending. For the most important minor groove-inward sections, the 'second best' motifs evident here are composed mostly of G|C nucleotides, the SHL ±2.5 AGGGG, SHL ±0.5 GGGGA and SHL ±3.5 AGGGA elements common to the second and third most stable constructs in our study, NCP-601

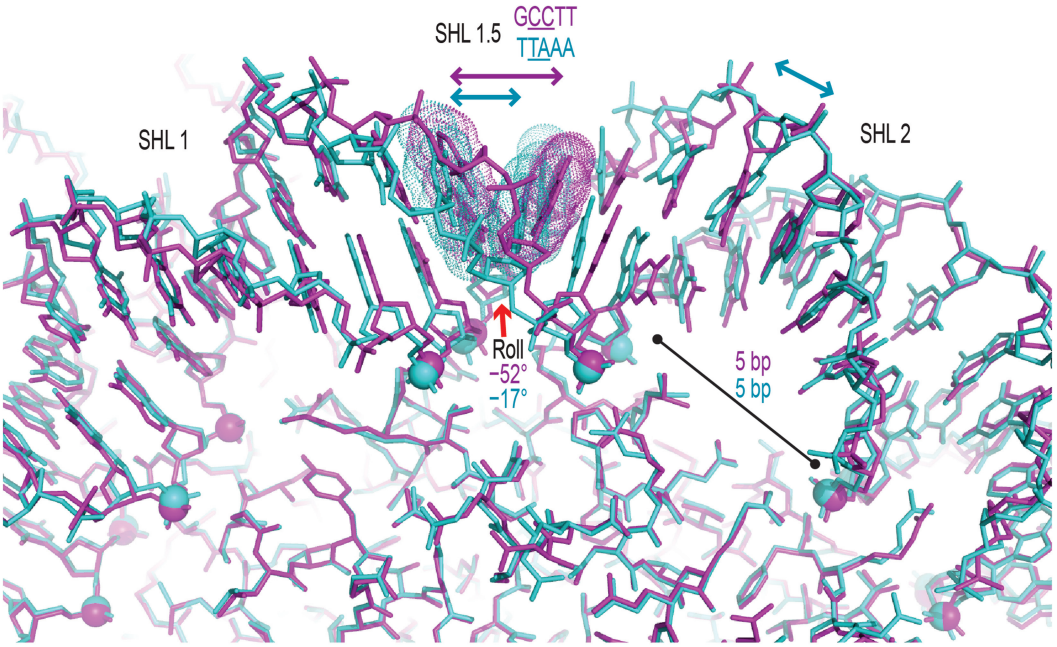

Figure 9. The intrinsic conformation of the DNA sequence dictates the structural changes required for histone association. NCP145 (magenta) and NCP-TA2 (cyan) both undergo DNA stretching around SHL 1 to SHL 2, but differ in DNA sequence over the SHL ± 1.5 region. The extreme kinking at GG = CC (bases, space-filling dots; roll = −52°, rise = 5.7 Å) in NCP145 serves to massively elongate (stretch, double-headed arrows) the DNA and simultaneously narrow the minor groove of the G|C-rich element, GCCTT. In contrast, however, the TTAAA element of NCP-TA2 has an intrinsically narrow minor groove (compare SHL 1.5 phosphodiester backbone regions facing viewer) and therefore only exhibits a modest stretch-associated kink at TA (bases, space-filling dots; roll = −17°, rise = 4.2 Å) as the minor groove would otherwise be overly narrow for histone association of the binding platform (phosphorous atoms, spheres). The remainder of the DNA stretch for NCP-TA2 is distributed over several dinucleotides towards SHL 2.

and NCP-601R (Figure 1B). Moreover, the H3–H4 tetramer binding sequences of the non-601 (α-satellite) constructs are also largely G|C, composed predominantly of the same step types, GG = CC, AG = CT and GA = TC, in addition to GC. Without consideration of specific sequence context, these dinucleotide types appear less flexible than pyrimidine–purine steps with respect to minor groove bending (30,31). However, together with AG = CT, the G|C steps are the most flexible towards shift (in order of decreasing flexibility: CG, GG = CC, AG = CT, GC) (35). Although GA = TC is ranked as the least shift-flexible step type, it displays an average shift value (−0.28 ± 0.46 Å for GA) of greater magnitude than any of the other step types (35). In this regard, it is important to note that the phases of the alternating shift patterns in the minor groove-inward regions appear to be conserved (Figure 3B) and thus constrained by histone binding, meaning that a shift-rigid step like GA = TC can also contribute favourably when appropriately positioned. Indeed, the GA steps in NCP-601L, NCP147 and NCP146b tend to adopt only negative shift values that are on average −0.47 ± 0.58 Å (the corresponding value for GG steps is by comparison 0.07 ± 0.70 Å), and in this way, they can support minor groove bending especially at the periphery of minor groove-inward regions, such as that at the NCP-601L SHL ±2.5 CTAGA or NCP146b ± 1.5 AGGGA motif. In this manner, shift-flexible as well as shift-biased dinucleotide steps in G|C-rich motifs can work cooperatively to allow favourable transition into a specialized form of minor groove bending (Figure 8).

The mechanical model and DNA sequence dependencies presented here provide a new scheme for understanding nucleosome structure, dynamics and stability. For instance, considering the specific constraints imposed by protein association together with conformational preferences of polynucleotide elements (e.g. five base pair sections) would yield improved methods for predicting histone octamer-DNA affinity. In addition, the ability to design tailored high affinity histone octamer binding sequences from knowledge of the rules governing stability will assist the next generation of studies on nucleosomal assemblies.

ACCESSION NUMBERS

Atomic coordinates and structure factors have been deposited in the Protein Data Bank under accession codes 3UT9, 3UTA and 3UTB.

SUPPLEMENTARY DATA

Supplementary Data are available at NAR Online: Supplementary Figures 1–4.

ACKNOWLEDGEMENTS

C.A.D. dedicates this work to the memory of Jonathan Widom, we remain inspired by his passion and intellect.

We are grateful to M. Wang, C. Schulze-Briese, V. Olieric, A. Pauluhn, T. Tomizaki, M. Fuchs, R. Bingel-Erlenmeyer, G. Pompidor and C. Rajendran for exceptional support at the Swiss Light Source (Paul Scherrer Institute, Villigen, Switzerland). E.Y.D.C carried out crystallographic work on NCP-601L and NCP-TA2 and conducted DNA footprinting, stability measurements and data analysis; D.V. carried out crystallographic work on NCP-601L, grew crystals of NCP-TA2 and conducted stability measurements; G.E.D provided expertise on DNA footprinting and conducted DNA production for NCP-TA2; B.W. grew crystals of and collected X-ray data for NCP146b; C.A.D. conducted structure solution and analysis and wrote the manuscript.

FUNDING

Academic Research Council, Ministry of Education, Singapore (grant 19/08); National Medical Research Council, Ministry of Health, Singapore. Funding for open access charge: NMRC/1312/2011.

Conflict of interest statement. None declared.

REFERENCES

1. Sadeh,R. and Allis,C.D. (2011) Genome-wide ''re''-modeling of nucleosome positions. *Cell*, **147**, 263–266.
2. Valouev,A., Johnson,S.M., Boyd,S.D., Smith,C.L., Fire,A.Z. and Sidow,A. (2011) Determinants of nucleosome organization in primary human cells. *Nature*, **474**, 516–520.
3. Widom,J. (2001) Role of DNA sequence in nucleosome stability and dynamics. *Q. Rev. Biophys.*, **34**, 269–324.
4. Davey,C.A., Sargent,D.F., Luger,K., Maeder,A.W. and Richmond,T.J. (2002) Solvent mediated interactions in the structure of the nucleosome core particle at 1.9 Å resolution. *J. Mol. Biol.*, **319**, 1097–1113.
5. Richmond,T.J. and Davey,C.A. (2003) The structure of DNA in the nucleosome core. *Nature*, **423**, 145–150.
6. Travers,A.A. (2004) The structural basis of DNA flexibility. *Philos. Transact. A Math. Phys. Eng. Sci.*, **362**, 1423–1438.
7. Tillo,D. and Hughes,T.R. (2009) G+C content dominates intrinsic nucleosome occupancy. *BMC Bioinformatics*, **10**, 442.
8. Tillo,D., Kaplan,N., Moore,I.K., Fondufe-Mittendorf,Y., Gossett,A.J., Field,Y., Lieb,J.D., Widom,J., Segal,E. and Hughes,T.R. (2010) High nucleosome occupancy is encoded at human regulatory sequences. *PLoS One*, **5**, e9129.
9. Fernandez,A.G. and Anderson,J.N. (2007) Nucleosome positioning determinants. *J. Mol. Biol.*, **371**, 649–668.
10. Wu,B., Mohideen,K., Vasudevan,D. and Davey,C.A. (2010) Structural insight into the sequence dependence of nucleosome positioning. *Structure*, **18**, 528–536.
11. Ong,M.S., Richmond,T.J. and Davey,C.A. (2007) DNA stretching and extreme kinking in the nucleosome core. *J. Mol. Biol.*, **368**, 1067–1074.
12. Vasudevan,D., Chua,E.Y. and Davey,C.A. (2010) Crystal structures of nucleosome core particles containing the '601' strong positioning sequence. *J. Mol. Biol.*, **403**, 1–10.
13. Luger,K., Rechsteiner,T.J. and Richmond,T.J. (1999) Preparation of nucleosome core particle from recombinant histones. *Meth. Enzymol.*, **304**, 3–19.
14. Wu,B., Davey,G.E., Nazarov,A.A., Dyson,P.J. and Davey,C.A. (2011) Specific DNA structural attributes modulate platinum anticancer drug site selection and cross-link generation. *Nucleic Acids Res.*, **39**, 8200–8212.
15. Leslie,A.G. (2006) The integration of macromolecular diffraction data. *Acta Crystallogr. D Biol. Crystallogr.*, **62**, 48–57.
16. Collaborative Computational Project, Number 4. (1994) The CCP4 suite: programs for protein crystallography. *Acta Crystallogr. D Biol. Crystallogr.*, **50**, 760–763.
17. Thåström,A., Bingham,L.M. and Widom,J. (2004) Nucleosomal locations of dominant DNA sequence motifs for histone-DNA interactions and nucleosome positioning. *J. Mol. Biol.*, **338**, 695–709.
18. Lu,X.J. and Olson,W.K. (2003) 3DNA: a software package for the analysis, rebuilding and visualization of three-dimensional nucleic acid structures. *Nucleic Acids Res.*, **31**, 5108–5121.
19. Zheng,G., Lu,X.J. and Olson,W.K. (2009) Web 3DNA—a web server for the analysis, reconstruction, and visualization of three-dimensional nucleic-acid structures. *Nucleic Acids Res.*, **37**, W240–W246.
20. Lavery,R. and Sklenar,H. (1988) The definition of generalized helicoidal parameters and of axis curvature for irregular nucleic acids. *J. Biomol. Struct. Dyn.*, **6**, 63–91.
21. Oohara,I. and Wada,A. (1987) Spectroscopic studies on histone-DNA interactions. I. The interaction of histone (H2A, H2B) dimer with DNA: DNA sequence dependence. *J. Mol. Biol.*, **196**, 389–397.
22. Luger,K., Rechsteiner,T.J., Flaus,A.J., Waye,M.M. and Richmond,T.J. (1997) Characterization of nucleosome core particles containing histone proteins made in bacteria. *J. Mol. Biol.*, **272**, 301–311.
23. Park,Y.J., Dyer,P.N., Tremethick,D.J. and Luger,K. (2004) A new fluorescence resonance energy transfer approach demonstrates that the histone variant H2AZ stabilizes the histone octamer within the nucleosome. *J. Biol. Chem.*, **279**, 24274–24282.
24. Maxam,A.M. and Gilbert,W. (1980) Sequencing end-labeled DNA with base-specific chemical cleavages. *Meth. Enzymol.*, **65**, 499–560.
25. Tan,S. and Davey,C.A. (2011) Nucleosome structural studies. *Curr. Opin. Struct. Biol.*, **21**, 128–136.
26. Lowary,P.T. and Widom,J. (1998) New DNA sequence rules for high affinity binding to histone octamer and sequence-directed nucleosome positioning. *J. Mol. Biol.*, **276**, 19–42.
27. Makde,R.D., England,J.R., Yennawar,H.P. and Tan,S. (2010) Structure of RCC1 chromatin factor bound to the nucleosome core particle. *Nature*, **467**, 562–566.
28. Olson,W.K. and Zhurkin,V.B. (2011) Working the kinks out of nucleosomal DNA. *Curr. Opin. Struct. Biol.*, **21**, 348–357.
29. Krueger,A., Protozanova,E. and Frank-Kamenetskii,M.D. (2006) Sequence-dependent base pair opening in DNA double helix. *Biophys. J.*, **90**, 3091–3099.
30. Balasubramanian,S., Xu,F. and Olson,W.K. (2009) DNA sequence-directed organization of chromatin: structure-based computational analysis of nucleosome-binding sequences. *Biophys. J.*, **96**, 2245–2260.
31. Morozov,A.V., Fortney,K., Gaykalova,D.A., Studitsky,V.M., Widom,J. and Siggia,E.D. (2009) Using DNA mechanics to predict in vitro nucleosome positions and formation energies. *Nucleic Acids Res.*, **37**, 4707–4722.
32. Tolstorukov,M.Y., Colasanti,A.V., McCandlish,D.M., Olson,W.K. and Zhurkin,V.B. (2007) A novel roll-and-slide mechanism of DNA folding in chromatin: implications for nucleosome positioning. *J. Mol. Biol.*, **371**, 725–738.
33. Hall,M.A., Shundrovsky,A., Bai,L., Fulbright,R.M., Lis,J.T. and Wang,M.D. (2009) High-resolution dynamic mapping of histone-DNA interactions in a nucleosome. *Nat. Struct. Mol. Biol.*, **16**, 124–129.
34. Hayatsu,H. and Ukita,T. (1967) The selective degradation of pyrimidines in nucleic acids by permanganate oxidation. *Biochem. Biophys. Res. Commun.*, **29**, 556–561.
35. Olson,W.K., Gorin,A.A., Lu,X.J., Hock,L.M. and Zhurkin,V.B. (1998) DNA sequence-dependent deformability deduced from protein-DNA crystal complexes. *Proc. Natl Acad. Sci. USA*, **95**, 11163–11168.
36. Segal,E. and Widom,J. (2009) Poly(dA:dT) tracts: major determinants of nucleosome organization. *Curr. Opin. Struct. Biol.*, **19**, 65–71.